Iterative SAFT Reconstruction for Manually Acquired Ultrasonic Measurement Data in Nondestructive Testing

Sayako Kodera
Ilmenau University of Technology
P. O. Box 100565, D-98684 Ilmenau, Germany
Email: sayako.kodera@tu-ilmenau.de

***Abstract* — Although ultrasonic testing (UT) still requires a lot of manual operations, reliability of manual UT has remained highly dependent on human factors. However, a measurement assistance system makes manual UT reproducible, opening up the possibility of post-processing the measurement data to further increase the inspection reliability. Nevertheless, manual UT is prone to systematic errors which degrade the reconstruction quality significantly. This study concerns a possible solution to handle positional inaccuracy for SAFT reconstruction. In an attempt to reduce artefacts in reconstruction, we aim to correct the positional information and modify the reconstruction system with its spatial approximation in an iterative manner. Through simulations, we have found the position dependency of the method and derived countermeasures. Example reconstruction results are provided, which demonstrate the validity of the proposed method.**

***Index Terms*—Nondestructive testing, Ultrasonic testing, SAFT, Manual measurement, Positional inaccuracy**

I. Introduction

Ultrasonic testing (UT) is a nondestructive testing method to inspect structure of test objects without inducing damage. Conventionally, an UT inspection requires either manual operation by a human technician or automated measurement systems. In manual UT, where a human technician observes the change in the echoed pulse, its inspection quality is highly dependent on the expertise of the technician [1]. In automatic UT, on the other hand, measurement data and the corresponding scan positions are recorded, which enables to visualize the inner structure of the test object and further process the data to improve the imaging quality, leading to more reliable inspection quality than its manual counterpart.

Nevertheless, there are still needs for manual UT, when, for instance, a complex structure is inspected, and its inspection reliability has been of great concern. In order to improve the inspection reliability of manual UT, an assistance system can be employed, which records measurement data and recognizes the scan positions through a tracking system. This allows us not only to visualize the measurement data but also to process it further for the better imaging quality [2].

Although their application to manual UT data has been typically excluded, several post-processing techniques have been developed and extensively employed for automatic UT data [3] [4] [5]. While the authors of [5] apply the signal processing methods widely used in the telecommunication field to the UT data, one of the well established post-processing method is the synthetic aperture focusing technique (SAFT) [3] [4]. The aim of SAFT is to improve the spatial resolution through performing superposition with respect to the propagation time delay [6]. In other words, SAFT regards the measurement region-of-interest (ROI) as a single aperture and each measurement as its spatial sampling, which indicates that the SAFT reconstruction requires accurate positional information.

However, the application of such techniques to manual UT data is so far little studied [7] [2]. The authors of [2] demonstrate the possibilities of utilizing post-processing with manual measurement data, yet the reconstruction quality is, compared to the reconstruction results of automatic measurement data, significantly degraded. Previously, we identified the possible error sources for such degradation and revealed that several systematic errors, such as varying contact pressure or inaccurate positional information due to the tracking error, can lead to strong artefacts formation [8]. Since such errors are inevitable in manual measurement, finding the way to reduce those artefacts could improve the reconstruction quality. Unlike other possible error factors which should be entirely estimated from the measurement data, the tracking error can be handled to some extent, as the positional information is, whether accurate or not, available.

Our goal in this study is to reduce the position-inaccuracy induced artefacts by correcting the measurement positions and adjusting the reconstruction system accordingly. So far, we are unaware of any other works that deal with this topic. However, expressing the reconstruction process mathematically enables us to approximate the correct model with regard to measurement positions, whereas the traditional regression approaches provide us a tool to estimate the tracking error from the available information. As a possible solution for proper handling of positional inaccuracy, we propose an iterative method combining these mathematical tools, which can be incorporated into reconstruction system.

II. Data model

A. Pulse-Echo Setup

For a measurement setup, we consider a manual contact testing where a handheld transducer is placed directly on the specimen surface at a position $\boldsymbol{p} \in \mathbb{R}^{\mathrm{K}}$.The transducer inserts an ultrasonic pulse $h(t)$ into a specimen and receives the reflected pulse, A-Scan, $a_{\boldsymbol{p}}(t)$ at the same position $\boldsymbol{p}$. The specimen is assumed to be homogenous and isotropic with the constant speed of sound c_0 and have a flat surface. During the measurement, the contact pressure is considered to be constant so that in the measurement data there is no temporal shift or amplitude change caused by improper coupling. The measurement position $\boldsymbol{p}$ is arbitrarily selected on the specimen surface and we suppose that there is at least one scatterer inside the specimen, which is regarded as point source.

The measured A-Scan $a_{\boldsymbol{p}}(t)$ can be considered as a convolution of the inserted pulse and the reflectivity of the specimen

$$a_{\boldsymbol{p}}(t) = h(t) * r(t) + n(t). \tag{1}$$

$r(t)$ denotes the reflectivity of the specimen and $n(t)$ the additive measurement noise, respectively, which is assumed to be zero-mean i.i.d. Gaussian noise with variance σ_N^2.

Conventionally, the inserted pulse $h(t)$ is modeled as a real-valued Gabor function [9], as

$$h(t) = e^{-\alpha t^2} \cdot \cos(2\pi f_C t + \phi), \tag{2}$$

where f_C, α and ϕ are the carrier frequency, the window width factor and the phase, respectively.

Since we consider the scatterers as point sources, the reflectivity $r(t)$ can be expressed as a sum of time-shifted delta for all I scatterers as

$$r(t;\tau) = \sum_{i=1}^{I} \beta_{\boldsymbol{p},i} \cdot \delta(t - \tau_i). \tag{3}$$

$\beta_{\boldsymbol{p},i}$ is the reflection coefficient for the position $\boldsymbol{p}$ and a scatterer s_i, whereas τ_i is the time-of-flight (ToF) which the ultrasonic pulse needs to travel for way forth and back from $\boldsymbol{p}$ to s_i. The ToF can be obtained with

$$\tau_i(\boldsymbol{p}) = \frac{2}{c_0} \cdot \|\boldsymbol{s}_i - \boldsymbol{p}\|_2 , \tag{4}$$

where $\|\boldsymbol{s}_i - \boldsymbol{p}\|_2$ the ℓ-2 norm of $\boldsymbol{s}_i$ and $\boldsymbol{p}$. Eq. (4) shows that the ToF depends on the position of both measurement and the scaterrer, resulting in the reflectivity as a function of time t and position $\boldsymbol{p}$ as well.

By inserting (3) into (1), we obtain the A-Scan as the time-shifted input pulse as

$$a(t;\boldsymbol{p}) = \sum_{i=1}^{I} \beta_{\boldsymbol{p},i} \cdot h(t - \tau_i(\boldsymbol{p})) + n(t). \tag{5}$$

Since we process the data digitally with the sampling interval of $\mathrm{d}t = \frac{1}{f_S}$, (5) becomes

$$a(t;\boldsymbol{p}) = \sum_{m=1}^{\mathrm{M}} \sum_{i=1}^{\mathrm{I}} \beta_{\boldsymbol{p},i} \cdot h(m\,\mathrm{d}t - \tau_i(\boldsymbol{p})) + n(m\,\mathrm{d}t), \tag{6}$$

where M is the number of temporal samples.

B. Forward Model with SAFT

The goal of SAFT reconstruction is to determine the location of scatterers in a solid test object. As (4) indicates, the distance between the scatterer and the measurement position, $\|\boldsymbol{s}_i - \boldsymbol{p}\|_2$, can be obtained through the ToF, suggesting that s_i is likely to be on the semicircle with $\boldsymbol{p}$ in the center and the radius of $\|\boldsymbol{s}_i - \boldsymbol{p}\|_2$. By computing such semicircles at different scan positions, we can specify the position of s_i. Based on this idea, SAFT extracts the ToF information, performs the superposition of the multiple measurement data and achieves a spatial focus [6].

In order to compute SAFT efficiently, it is desirable to express (6) as a linear transform. As (6) demonstrates, the obtained A-Scan can be modeled as a sum of the time-shifted input pulse $h(t)$, enabling to form a matrix $\boldsymbol{H}(\boldsymbol{p})$ from the impulse response at the measurement position $\boldsymbol{p}$ for all possible scatterer positions. We call $\boldsymbol{H}(\boldsymbol{p})$ a SAFT matrix which is tied to the measurement position and has a dimension of $\mathbb{R}^{\mathrm{M} \times \mathrm{L}}$, when there are L possible scatterer positions in our ROI. A column vector of the SAFT matrix $\boldsymbol{h} \in \mathbb{R}^{\mathrm{M}}$ can be expressed as

$$[\boldsymbol{H}(\boldsymbol{p})]_{(:,l)} = \boldsymbol{h}_l(\boldsymbol{p}) = \sum_{m=1}^{\mathrm{M}} \beta_{\boldsymbol{p},l} \cdot h(m\,\mathrm{d}t - \tau_l(\boldsymbol{p})), \tag{7}$$

where l is the column index which corresponds to the scatterer positions. This allows us to rewrite (6) as a linear transform

$$\boldsymbol{a}(\boldsymbol{p}) = \boldsymbol{H}(\boldsymbol{p}) \cdot \boldsymbol{b} + \boldsymbol{n} = \hat{\boldsymbol{a}}(\boldsymbol{p}) + \boldsymbol{n} \tag{8}$$

where $\boldsymbol{a}(\boldsymbol{p}) \in \mathbb{R}^{\mathrm{M}}$, $\hat{\boldsymbol{a}}(\boldsymbol{p}) \in \mathbb{R}^{\mathrm{M}}$ and $\boldsymbol{n} \in \mathbb{R}^{\mathrm{M}}$ are the A-Scan, its model and the measurement noise, respectively, as vector form and $\boldsymbol{b} \in \mathbb{R}^{\mathrm{L}}$ is the vectorized "defect map" which represents the scatterer positions [10]. When there is only one scatterer located at the l-th position of our ROI, each element of the vectorized defect map b_q can be expressed as

$$b_q = \begin{cases} \beta_{\boldsymbol{p},l}, & \text{for } q = l \\ 0 & \text{else} \end{cases}, \tag{9}$$

where the index q satisfies $q = 1, 2, ..., \mathrm{L}$. Consequently, SAFT reconstruction becomes the following optimization problem [10]

$$\min_{\boldsymbol{b}} \|\boldsymbol{a}(\boldsymbol{p}) - \boldsymbol{H}(\boldsymbol{p}) \cdot \boldsymbol{b}\|_2. \tag{10}$$

III. Methods

Since the inaccurate positional information can lead the SAFT matrix to fail in proper modeling of the measured A-scan, the quality of the SAFT reconstruction strongly depends on the accuracy of the input measurement positions. Suppose an A-Scan $\boldsymbol{a}(\boldsymbol{p})$ is taken at the position $\boldsymbol{p} \in \mathbb{R}^{\mathrm{K}}$, and the tracking system recognizes the measurement position as $\hat{\boldsymbol{p}} = \boldsymbol{p} + \Delta\boldsymbol{p}$ with the tracking error $\Delta\boldsymbol{p}$. Based on this falsely recognized measurement position $\hat{\boldsymbol{p}}$, we compute a SAFT matrix $\boldsymbol{H}(\hat{\boldsymbol{p}})$ which corresponds to an incorrect A-Scan model $\hat{\boldsymbol{a}}(\hat{\boldsymbol{p}})$. When the deviation between $\hat{\boldsymbol{a}}(\hat{\boldsymbol{p}})$ and the correct A-Scan model $\hat{\boldsymbol{a}}(\boldsymbol{p})$ is large, reconstructing the measurement

data $\boldsymbol{a}(\boldsymbol{p})$ with the improper SAFT matrix $\boldsymbol{H}(\hat{\boldsymbol{p}})$ results in a significant degradation of reconstruction quality.

For improving the reconstruction quality despite the positional inaccuracy, it is essential to bridge the gap between the proper SAFT matrix $\boldsymbol{H}(\boldsymbol{p})$ and the falsely computed matrix $\boldsymbol{H}(\hat{\boldsymbol{p}})$, such that the resulting A-Scan model becomes very similar to the correct model. In order to minimize the deviation in A-Scan modeling, we aim to approximate the correct SAFT matrix from the available information, i.e. the measurement data $\boldsymbol{a}(\boldsymbol{p})$ and the positional information $\hat{\boldsymbol{p}}$. This is done based on the first Taylor approximation of the function f

$$\begin{aligned} f(u) &\approx f(v) + f'(v) \cdot (u - v) \\ &\approx f(v) - f'(v) \cdot (v - u), \end{aligned} \tag{11}$$

where $f(u)$ for u near v can be approximated with $f(v)$ and its derivative $f'(v)$ when $|u - v| \ll u$.

In the following subsections, the spatial approximation of the SAFT matrix is firstly derived (Sec.III.A), and an iterative method, which estimates the tracking error $\Delta\boldsymbol{p}$ and improves the positional accuracy, is presented (Sec.III.B). Although SAFT matrix is meant to be used for solving the optimization problem shown in (10), in this section we will be focusing on modeling A-Scan properly by assuming that the position of scatterers, i.e. the defect map $\boldsymbol{b}$, is known. Moreover, for the sake of simplicity we consider a noise free scenario, i.e. the obtained measurement data $\boldsymbol{a}(\boldsymbol{p})$ becomes identical to our A-Scan model $\hat{\boldsymbol{a}}(\boldsymbol{p})$.

A. Spatial Approximation of SAFT Matrix

In order to obtain a spatial approximation of SAFT matrix, we should model A-Scans in terms of measurement positions, which is, as (2), (4) and (6) suggest, a non-linear transformation $f : \boldsymbol{p} \in \mathbb{R}^{\mathrm{K}} \rightarrow f(\boldsymbol{p}) \in \mathbb{R}^{\mathrm{M}}$. Yet, this non-linear transformation can be considered as a superposition of each scatterer position in the same manner we model an A-Scan in (6), resulting in the non-linear transformation for a single scatterer becoming identical to the corresponding column of the SAFT matrix as

$$f_i(\boldsymbol{p}) = \boldsymbol{h}_l(\boldsymbol{p}) = \boldsymbol{H}(\boldsymbol{p}) \cdot \boldsymbol{b}^{(l)}. \tag{12}$$

f_i denotes the non-linear transformation of the measurement position $\boldsymbol{p}$ for the i-the scatterer which is located at the l-th position in our ROI and $\boldsymbol{h}_l$ is the corresponding l-th column vector of the SAFT matrix. $\boldsymbol{b}^{(l)}$ is a vectorized defect map containing only one non-zero element, e.g. 1, in the l-th row.

When we consider the positional error $\Delta\boldsymbol{p}$ in a small range, i.e. $\Delta\boldsymbol{p} \ll \boldsymbol{p}$, $\boldsymbol{h}_l$ becomes locally linear and can be linearly approximated as

$$\boldsymbol{h}_l(\boldsymbol{p}) \approx \boldsymbol{h}_l(\boldsymbol{p} + \Delta\boldsymbol{p}) - \boldsymbol{J}_{\boldsymbol{h}_l}(\boldsymbol{p} + \Delta\boldsymbol{p}) \cdot \Delta\boldsymbol{p}, \tag{13}$$

where $\boldsymbol{J}_{\boldsymbol{h}_l} \in \mathbb{R}^{\mathrm{M} \times \mathrm{K}}$ is the Jacobian matrix of $\boldsymbol{h}_l$, which can be expressed as

$$\boldsymbol{J}_{\boldsymbol{h}_l}(\boldsymbol{p}) = \left[\frac{\partial \boldsymbol{h}_l(\boldsymbol{p})}{\partial \boldsymbol{p}} \right]. \tag{14}$$

Since $\boldsymbol{J}_{\boldsymbol{h}_l}$ is associated with the l-th column of the SAFT matrix, we can form a comprehensive Jacobian matrix $\boldsymbol{J} \in \mathbb{R}^{\mathrm{M\,L} \times \mathrm{K}}$, in the similar manner as (8), which contains the derivative of $\boldsymbol{h}_l$ for all possible scatterer positions L as

$$\boldsymbol{J}(\boldsymbol{p}) = \left[\boldsymbol{J}_{\boldsymbol{h}_1}(\boldsymbol{p})^{\mathrm{T}} \boldsymbol{J}_{\boldsymbol{h}_2}(\boldsymbol{p})^{\mathrm{T}} ... \boldsymbol{J}_{\boldsymbol{h}_{\mathrm{L}}}(\boldsymbol{p})^{\mathrm{T}} \right]^{\mathrm{T}}. \tag{15}$$

Consequently, the inner product of $\boldsymbol{J}$ and $\Delta\boldsymbol{p}$ in (13) yields a vector $\in \mathbb{R}^{\mathrm{M\,L}}$, from which a matrix $\boldsymbol{D} \in \mathbb{R}^{\mathrm{M} \times \mathrm{L}}$ can be formed with inverse vec operation as

$$\begin{aligned} \boldsymbol{D}(\hat{\boldsymbol{p}}; \Delta\boldsymbol{p}) &= \mathrm{vec}^{-1}_{\mathrm{M,L}}\{\boldsymbol{J}(\hat{\boldsymbol{p}}) \cdot \Delta\boldsymbol{p}\} \\ &= \left[(\mathrm{vec}\{\boldsymbol{I}_{\mathrm{L}}\}^{\mathrm{T}} \otimes \boldsymbol{I}_{\mathrm{M}} \right] \cdot \left[\boldsymbol{I}_{\mathrm{L}} \otimes (\boldsymbol{J}(\hat{\boldsymbol{p}}) \cdot \Delta\boldsymbol{p}) \right]. \end{aligned} \tag{16}$$

Since $\boldsymbol{D}$ has the same dimension as our SAFT matrix $\boldsymbol{H}$, we can express $\boldsymbol{h}_l$ by applying the same approach in (8) to (13) as

$$\boldsymbol{h}_l(\boldsymbol{p}) \approx \boldsymbol{h}_l(\hat{\boldsymbol{p}}) - b_l \cdot \boldsymbol{d}_l(\hat{\boldsymbol{p}}; \Delta\boldsymbol{p}), \tag{17}$$

where b_l and $\boldsymbol{d}_l$ are the l-th element of $\boldsymbol{b}$ and the l-th column vector of $\boldsymbol{D}$, respectively. Inserting (12) and (17) into (13) yields

$$\boldsymbol{H}(\boldsymbol{p}) \cdot \boldsymbol{b}^{(l)} \approx [\boldsymbol{H}(\hat{\boldsymbol{p}}) - \boldsymbol{D}(\hat{\boldsymbol{p}}; \Delta\boldsymbol{p})] \cdot \boldsymbol{b}^{(l)}, \tag{18}$$

which indicates that we can approximate the correct SAFT matrix through the falsely computed SAFT matrix as

$$\boldsymbol{H}(\boldsymbol{p}) \approx \boldsymbol{H}(\hat{\boldsymbol{p}}) - \boldsymbol{D}(\hat{\boldsymbol{p}}; \Delta\boldsymbol{p}). \tag{19}$$

B. Iterative Position Correction

For properly approximating the correct SAFT matrix, (19) indicates that we need the information about the tracking error $\Delta\boldsymbol{p}$. However, as we only know the falsely tracked position $\hat{\boldsymbol{p}}$, the tracking error should be estimated from the obtained measurement data $\boldsymbol{a}(\boldsymbol{p})$ and the positional information $\hat{\boldsymbol{p}}$. Moreover, although our approximation is less susceptive to the positional error than just calculating a SAFT matrix at the wrong position, the validity range of our approximation is limited. In order to tackle these problems, we incorporate an iterative method into our approximation process, so that we can estimate the tracking error $\Delta\boldsymbol{p}$ and improve the positional accuracy. In this subsection, we consider a simple measurement scenario where there is only one scatterer located at the l-th position in our ROI, i.e. the measured A-Scan a is identical to $\boldsymbol{h}_l$, and measurements are taken along the x-axis.

Eq. (17) indicates that the tracking error can be estimated by comparing the measurement data and the falsely modeled A-Scan. Since the transducer is further assumed to be placed directly on the object surface with the constant contact pressure, the vertical component z becomes 0 and remains constant, resulting in a measurement position becoming $\boldsymbol{p} = [x, 0]$. This enables us to express both measured and modeled A-Scans as a function of x and remove the tracking error $\Delta\boldsymbol{p} = \Delta x$ from vec^{-1} operator in (16). As a result, (17) can be formulated with the model derivative $\dot{\boldsymbol{h}}_l$ into a least squares problem as

$$\min_{\Delta x} \|\boldsymbol{h}_l(\hat{x}) - \boldsymbol{h}_l(x) - \dot{\boldsymbol{h}}_l(\hat{x}) \cdot \Delta x\|_2, \tag{20}$$

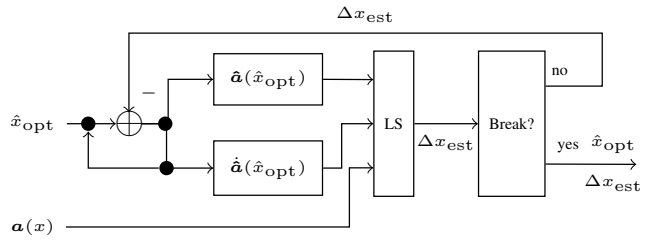

Figure 1: Block diagram of the iterative method to estimate and improve the positional error

through which we can obtain the estimated positional error Δx_{est}.

If we take into account this estimated error and update the positional information as $\hat{x}_{\mathrm{opt}} = \hat{x} - \Delta x_{\mathrm{est}}$, we can further reduce the positional error. With the improved scan position $\hat{x}_{\mathrm{opt}}$, (20) can be solved again, which provides a *new* estimated error, realizing the better approximation than the previous one with $\hat{x}$. In other words, repeating this procedure can improve the positional accuracy and consequently realize the reliable approximation for the SAFT matrix in (19).

This iterative process is depicted in Fig. 1. The breaking condition is either (a) the squared error of the approximated A-Scan $\tilde{\boldsymbol{a}}(\hat{x}_{\mathrm{opt}}; \Delta x_{\mathrm{est}})$ compared to the measured A-Scan $\boldsymbol{a}(x)$ (in our scenario, identical to the correct model $\hat{\boldsymbol{a}}(x)$) reaches the given target value or (b) the maximal number of iteration is carried out. After the iteration break, $\hat{x}_{\mathrm{opt}}$ and Δx_{est} are returned as output.

IV. Simulation I: Iterative Position Correction

Performance of the proposed method was examined through simulations where we applied the algorithm presented in III.B to simulated data sets. The goal of the simulations was to illustrate the error sensitivity of the proposed method, which can ultimately lead us to determine how we should incorporate our method into reconstruction process.

A. Assumptions and Test Parameters

For the simulations we chose an aluminum object for which we set the same assumptions as we described in Sec.II.A. For the sake of simplicity, the measurement data is regarded as noise free. Our ROI contains one scatterer and is a part of the test object where back and side wall echoes can be neglected. In order to illuminate the position-dependency of the results, the transducer is assumed to be ominidirectional. Table I provides a summary of the test parameters.

B. Evaluation Criterion and Variables

In order to evaluate the simulation results, we chose two criterion: the position correction and the approximation quality. The position correction $\Delta x_{\mathrm{opt}} = x - \hat{x}_{\mathrm{opt}}$ shows how close we can correct the position $\hat{x}$ through the proposed method. The approximation quality is assessed with the modified squared error $\mathrm{SE}^{\dagger}$ of the approximated A-Scan $\tilde{\boldsymbol{a}}(\hat{x}_{\mathrm{opt}}; \Delta x_{\mathrm{est}})$

Simulation	Parameter	Value
For both simulations	Speed of sound c_0	$6300\,\mathrm{m\,s^{-1}}$
	Carrier frequency f_C	5 MHz
	Wavelength λ	1.26 mm
	Bandwidth factor α	20 $(\mathrm{MHz})^2$
	Reflection coefficient c_x	1
	Sampling frequency f_S	80 MHz
	Sampling distance dz	39.375 µm
	ROI (L × H) $\mathrm{N}_x \times \mathrm{N}_z$	20 mm × 35 mm 40 × 880
	Scatterer position $\boldsymbol{s}$ (s_x, s_z)	(10 mm, 22.5 mm) (20 dx, 571 dz)
Simulation I	Opening angle	180° (omnidirectional)
	Scan positions	See Fig. 2
Simulation II	Opening angle	25°
	Scan positions	Equidistant
	sampling distance dx	0.5 mm
	Tracking error Δx	1.26 mm

Table I: Summary of the test parameters for the simulations

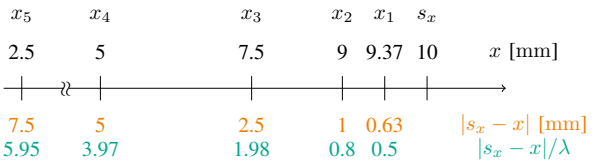

Figure 2: Illustration of the measurement positions used for the simulation I in relation to the scatterer position s_x

compared to the measurement data $\boldsymbol{a}(x)$. $\mathrm{SE}^{\dagger}$ can be expressed as

$$\mathrm{SE}^{\dagger} = \frac{\|\gamma\tilde{\boldsymbol{a}} - \boldsymbol{a}\|_2}{\|\boldsymbol{a}\|_2}, \tag{21}$$

where γ is a normalization factor obtained through

$$\gamma = \frac{\boldsymbol{a}^{\mathrm{T}} \cdot \tilde{\boldsymbol{a}}}{\tilde{\boldsymbol{a}}^{\mathrm{T}} \cdot \tilde{\boldsymbol{a}}}. \tag{22}$$

As we aimed to illustrate the error sensitivity of our method, the simulations were carried out with different tracking error Δx. Furthermore, since the measurement data is tied to its scan position, the error sensitivity is expected to vary with scan position x, which we set as our second variable in the simulations. Considering the symmetry in the measurement setup, we used the *scatterer-scan* distance, $|s_x - x|$, as a variable for x. Fig. 2 illustrates the measurement positions used in simulations. For the break condition, we set our target to $\mathrm{SE}^{\dagger} = 0.01$ and the maximal number of iterations to 15.

C. Results

Fig. 3a and Fig. 3b show the positional error correction and the squared error of the approximated A-Scan for four different measurement positions depicted in Fig. 2. In general, position-dependency can be well observed, and Fig. 3b shows that our approximation can tolerate the positional error for certain range.

When the measurement position is only $0.63\,\mathrm{mm}$, which is equivalent to half wavelength, away from the scatterer, the error up to -0.5λ can be well corrected, leading to successful approximations. However, when the error is within the range of -0.5λ and 1.5λ, the error is not corrected. This is because

there is almost no difference in the falsely computed A-Scan and the correct model. This no-correction range is related to the symmetry in the measurement setup, which results in the doubled width in the range. That is to say, in order for the error correction to successfully function, the deviation in A-Scan between the correct model and its falsely computed counterpart should be large enough. On the other hand, as the deviation in A-Scan is very little within the no-correlation range, the correct model can be very well approximated even without error correction. For the error above 0.5λ the difference in A-Scan becomes larger, prompting the error correction. Yet, the position is corrected to the opposite side of the measurement position with respect to the scatterer, where we can obtain the identical A-Scan model.

Likewise, for the measurement position which is $1\,\mathrm{mm}$ away from the scatterer we can observe both the correction and the no-correction range, and the both results show very similar progression, except two points. One is the "sudden" improvement in the error correction, when the error is equal to 0.76λ. This is because the scan position is now located further away from the scatterer than the previous result, making A-Scan modeling more sensitive to the error. As a result, the deviation in A-Scans becomes large enough to prompt the error correction. The other is the "sudden" worsening in the approximation with the error of 0.8λ, where the falsely tracked position is directly above the scatterer, i.e. $\hat{x} = s_x$. When an A-Scan is modeled directly above the scatterer, the progression in error sensitivity of A-Scan modeling becomes convex as shown in Fig. 4. Solving the least squares problem (20) based on $\hat{x} = s_x$ "optimizes" the position to s_x, failing to correct $\hat{x}$ to x. Since A-Scan modeling is more sensitive to the error than the previous result, the correct A-Scan model can be no longer well approximated without correcting the error.

On the contrary, as the measurement position moves away from the scatterer, the change in position results in the larger deviation in A-Scan, making the no-correction range negligible. Consequently, the error can be well corrected within the certain correction range. This correction range narrows with the increasing distance between the scatterer and the measurement position, since our approximation becomes more susceptive to the positional error. We've found that the positional error can be successfully corrected up to the first local minima after the global minimum (Fig. 4). In case of $|s_x - x| = 2.5\,\mathrm{mm}$, which is equivalent to 1.98λ, we can also observe that the error correction impairs when $\hat{x}$ approaches to s_x.

Above all, the obtained results show that the proposed method could improve the accuracy of A-scan modeling with the inaccurate positional information, which ultimately leads us to a better SAFT reconstruction. In order to assure the reconstruction quality, we should find the proper countermeasures for the no-correction range and the error sensitivity which increases with the measurement-scatterer distance.

For the no-correction range, we could set the threshold $\mathrm{SE}^{\dagger}_{\mathrm{th}}$ to initiate the error correction. Since the deviation in A-Scan is very little within the no-correction range, there is very likely no need for the approximation. When $\mathrm{SE}^{\dagger}$ of the falsely computed A-scan is smaller than $\mathrm{SE}^{\dagger}_{\mathrm{th}}$, then the modeled A-Scan, as well as the corresponding SAFT matrix, will remain unchanged, which reduces the overall computational time. When $\mathrm{SE}^{\dagger} > \mathrm{SE}^{\dagger}_{\mathrm{th}}$ and $\mathrm{SE}^{\dagger}$ of the resulting approximation is not well improved, which is very likely the case where the tracked position is directly above the scatterer, then this data can be discarded.

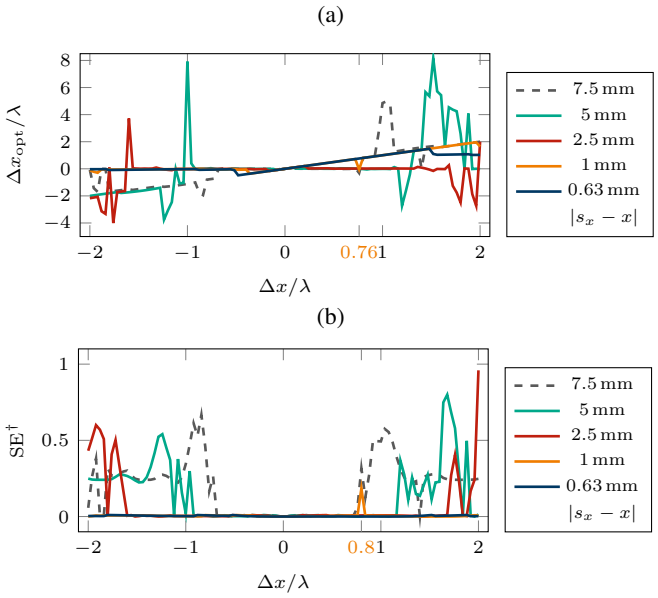

Figure 3: Results obtained with simulation I: (a) position correction normalized with the wavelength λ and (b) normalized squared error of the approximated A-Scans compared to their correct models

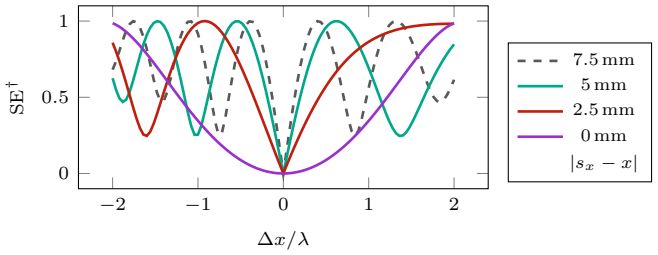

Figure 4: Error sensitivity of A-Scan modeling at different scan positions

In order to tackle the increasing error sensitivity with the scatterer-scan distance, it is desirable to suppress the contribution of the measurement data taken at the position far away from the scatterer.For this purpose, we can apply a spatial filter which varies the reflection coefficients according to the positions. A proper filter can be selected through comparing the measurement data with its neighboring data. When the change in the measurement data is large, which indicates that the position is located far away from the scatterer, we can accordingly choose the smaller reflection coefficient. In fact, transducers employed in real measurements have a limited angular sensitivity range which can be regarded as a form of spatial filters.

V. Simulation II: Reconstruction with Iterative Position Correction

A. Simulation Setup

In order to verify the proposed method, an example measurement data set is reconstructed. The same assumptions as the simulation I are made, and a summary of the test parameters are provided in Table I. We selected the transducer opening angle as a substitution of a spatial filter, which makes the scatterer *invisible* from the scan positions more than $5\,\mathrm{mm}$ away from the scatterer. Each measurement data is considered to be taken at a measurement grid point. The tracking system is, on the other hand, assumed to be capable of providing the positional information between two grid points. With that said, the tracking error is regarded not as quantization error but as mere false recognition due to, for instance, the sudden move of the transducer. Initially, the SAFT matrix is pre-calculated for all measurement grid points based on *a priori* knowledge regarding the test object.

The simulations are carried out with the following steps: first, the measurement data is taken at a particular grid point x which is recognized as $\hat{x}$. When the reconstruction process is accompanied with position correction, $\hat{x}$ is corrected to $\hat{x}_{\mathrm{opt}}$, and the SAFT matrix is modified accordingly, whereas without correction both $\hat{x}$ and the SAFT matrix remain same. Then, either $\hat{x}$ or $\hat{x}_{\mathrm{opt}}$ is rounded to the nearest grid point at which the obtained measurement data is stored in the system. After completing the measurement, the stored data is reconstructed.

B. Results

Fig. 5 shows the simulation results. As a reference, the measurement data (Fig. 5a) is stored in the system at the correct positions and reconstructed with the pre-calculated SAFT reconstruction matrix (Fig. 5b). When the positional information is incorrect and, as a result, A-Scans are assigned to the false positions to be stored in the system, the resulting data becomes incomplete and incoherent (Fig. 5c), which degrades the quality of the reconstruction with the given SAFT matrix (Fig. 5d). However, when the tracked positions are corrected with the proposed method and the SAFT matrix is modified, more A-Scans are assigned to the correct positions (Fig. 5e), and the reconstruction quality is significantly improved (Fig. 5f).

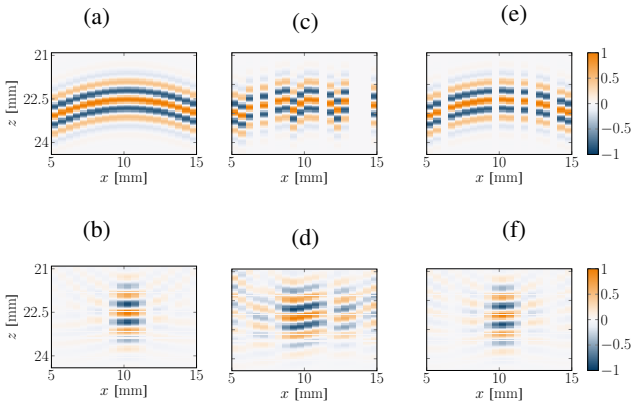

Figure 5: Results obtained with simulation II: (a) measurement data at the correct positions, (b) reference reconstruction, (c) measurement data according to the tracked positions with the tracking error of $1.26\,\mathrm{mm}$, (d) reconstruction of the measurement data, (e) measurement data after position correction, (f) reconstruction of the position-corrected measurement data

VI. Conclusions

In this study, a possible solution to handle positional inaccuracy for SAFT reconstruction was presented. We have derived the spatial approximation of SAFT reconstruction matrix and proposed an iterative process to improve positional accuracy. The performance of the proposed method was examined through simulations, revealing two major problems to overcome for incorporating this approach into reconstruction process. First, for successful error correction the deviation between the falsely computed A-Scan model and the measurement data should be large enough. This suggests that we should initiate error correction, only when the deviation in A-Scan is large enough. Second, the proposed method becomes susceptive to positional error when the scan position moves away from a scatterer. As a countermeasure, we can apply a spatial filter to suppress the contribution of the measurement data taken far away from the scatterer. Based on these findings, an example measurement data set was reconstructed, in which artefacts are significantly reduced with the proposed method.

References

[1] P. Cawley. Non-destructive testing - current capabilities and future directions. *Proceedings of the Institution of Mechanical Engineers, Part L*, vol 215, 2001.

[2] F. Krieg, S. Lugin, J. Kirchhof, A. Ihlow, T. Schwender, G. del Galdo, F. Römer, and A. Osman. Saft processing for manually acquired ultrasonic measurement data with 3D smartinspect. 2018. SHM-NDT.

[3] T.E. Hall, L.D. Reid, and S.R. Doctor. The SAFT-UT Real-Time Inspection System - Operational Principles and Implementation. Technical report, Pacific Northwest Laboratory, 1988.

[4] J. Krautkrämer and H. Krautkrämer. *Ultrasonic Testing of Materials*. Springer-Verlag, 1990.

[5] L. Ericsson and M.G. Gustafsson. Perception and Entropy Inspired Ultrasonic Grain Noise Suppression using Noncoherent Detector Statistics. In *ECNDT*, 1998.

[6] F. Lingvall. *Time-domain Reconstruction Methods for Ultrasonic Array Imaging*. PhD thesis, Uppsala University, 2004.

[7] K. Mayer, M. Ibrahim, M. Krause, M. Schubert. Requirements for a Small Size Ultrasonic Imaging System for Inspection of Concrete Elements. 2016. 19th World Conference on Non-Destructive Testing.

[8] F. Krieg, S. Kodera, J. Kirchhof, F. Römer, A. Ihlow, S. Lugin, A. Osman, and G. Del Galdo. 3D reconstruction of handheld data by SAFT and its impediment by measurement inaccuracies. In *IEEE IUS*, 2019. (To be published).

[9] R. Demirli and J. Saniie. Asymmetric Gaussian Chirplet Model for Ultrasonic Echo Analysis. *IEEE International Ultrasonics Symposium Proceedings*, 2010.

[10] J. Kirchhof, F. Krieg, F. Römer, A. Ihlow, A. Osman, and G. Del Galdo. Speeding up 3D SAFT for ultrasonic NDT by sparse deconvolution. In *IEEE IUS*, 2016.